We are IntechOpen, the world's leading publisher of Open Access books Built by scientists, for scientists

6,900
Open access books available

185,000
International authors and editors

200M
Downloads

Our authors are among the

154
Countries delivered to

TOP 1%
most cited scientists

12.2%
Contributors from top 500 universities



WEB OF SCIENCE™

Selection of our books indexed in the Book Citation Index in Web of Science™ Core Collection (BKCI)

Interested in publishing with us?
Contact book.department@intechopen.com

Numbers displayed above are based on latest data collected.
For more information visit www.intechopen.com



15

Nanophotonic Hierarchical Holograms: Demonstration of Hierarchical Applications Based on Nanophotonics

Naoya Tate et al.*
The University of Tokyo, Japan

1. Introduction

Recently, Italy's National Committee for Cultural Heritage found some microscopic codes in Mona Lisa's pupils by using a magnifying glass (Lorenzi, 2010). Experts have pointed out that the codes may represent several messages, including the initials of Leonardo Da Vinci, "*LV*". On the other hand, how and why such microscopic messages were embedded in her pupils has not been revealed yet. The most interesting part of this *other Da Vinci code* is that, although techniques for microscopic fabrication and retrieval had not been generally established in the early 16th century, the concept of embedding secret messages in a macro-scale view already existed—or as we now say, "The best place to hide a leaf is in a forest".

Present-day techniques for realizing this concept involve the ideas of *covertness* and *overtness*. The former means not showing something openly, and the latter means the opposite. As Da Vinci showed 500 years ago in Mona Lisa' s pupils, microscopic optical techniques are suitable for embedding secret messages in a macro-scale optical observation, because the hierarchical structure inherent between different levels of the optical scale can be implemented simply, and the levels are functionally independent of each other. For instance, confidential information can be hidden in any of the physical attributes of light, such as phase, wavelength, spatial frequency, or polarization, so that one kind of anti-counterfeiting is represented (Javidi et al., 1994; Refregier et al., 1995; Rakuljic et al., 1992).

Holography, which generates natural three-dimensional images consisting of a number of diffracted light beams, is one of the most common anti-counterfeiting optical techniques (Renesse et al., 1998). In the case of a volume hologram, the surface of the hologram is ingeniously designed into a complicated structure that diffracts incident light in specific directions. A number of diffracted light beams can form an arbitrary three-dimensional image. Because these structures are generally recognized as being difficult to duplicate,

* Makoto Naruse[1,2], Takashi Yatsui[1], Tadashi Kawazoe[1], Morihisa Hoga[3], Yasuyuki Ohyagi[3], Yoko Sekine[3], Tokuhiro Fukuyama[3], Mitsuru Kitamura[3] and Motoichi Ohtsu[1]
[1]*The University of Tokyo, Japan*
[2]*National Institute of Information and Communications Technology, Japan*
[3]*Dai Nippon Printing Co. Ltd., Japan*

holograms have been widely used in the anti-counterfeiting of bills, credit cards, etc. However, conventional anti-counterfeiting methods based on the physical appearance of holograms are less than 100% secure (McGrew et al., 1990). Although they provide ease of authentication, adding another security feature without causing any deterioration in the appearance is quite difficult.

Many existing optical devices and systems, not just holography, operate based on the phenomena of *propagating* light. Therefore, their performance is generally limited by the diffraction of light (Zhdanov et al., 1998). The critical difficulty in improving the function of conventional holograms is that they are also bounded by the diffraction limit. However, with recent advances in nanophotonics, especially in systems utilizing optical near-field interactions, several optical devices and systems can be designed at densities beyond those conventionally constrained by the diffraction limit (Ohtsu et al., 2008). Because several physical parameters of propagating light are not affected by nanometric structures, the conventional optical responses in the optical far-field are not affected by these structures either. Essentially, this means that another functional layer in the optical near-field regime can be added to conventional optical devices and systems without any effect on their primary quality, such as reflectance, absorptance, refractive index, or diffraction efficiency.

Here, we propose a *nanophotonic hierarchical hologram* as a typical demonstration of this concept. The nanophotonic hierarchical hologram is a functionally improved version of a conventional hologram that works in both the optical far- and near-fields (Tate et al., 2008). Moreover, a *nanophotonic code*, which is physically a subwavelength-scale shape-engineered metal nanostructure, is embedded in the hierarchical hologram to implement a near-mode function (Tate et al., 2010). In this chapter, the basic concept of the nanophotonic hierarchical hologram with embedded nanophotonic codes and the fabrication of a sample device are described. In particular, since the proposed approach involves embedding a nanophotonic code *within* the patterns of the hologram, which is basically composed of one-dimensional grating structures, clear polarization dependence is found compared with the case where it is not embedded within a hologram or an arrayed structure. There are also other benefits with the proposed approach: a major benefit is that the existing industrial facilities and fabrication technologies that have been developed for conventional holograms can be fully utilized, yet allowing novel functionalities to be added to the hologram.

2. Hierarchical nanophotonic system

2.1 Nanophotonics

Nanophotonics is a novel technology that utilizes the optical near-field, the electromagnetic field that mediates the interactions between closely spaced nanometric matter (Ohtsu et al., 2008). As shown in Fig. 1(a), optical near-fields are the elementary surface excitations on nanometric particles, which are induced by incident propagating light. By exploiting optical near-field interactions, nanophotonics has broken through the integration density restrictions imposed on conventional optical devices by the diffraction limit of light (Fig. 1(b)). This higher integration density has enabled realization of *quantitative* innovations in photonic devices and optical fabrication technologies (Nishida et al., 2007; Ozbay et al., 2006). Moreover, *qualitative* innovations have been accomplished by utilizing novel functions and phenomena made possible by optical near-field interactions that are otherwise unachievable with conventional propagating light (Ohtsu et al., 2008).

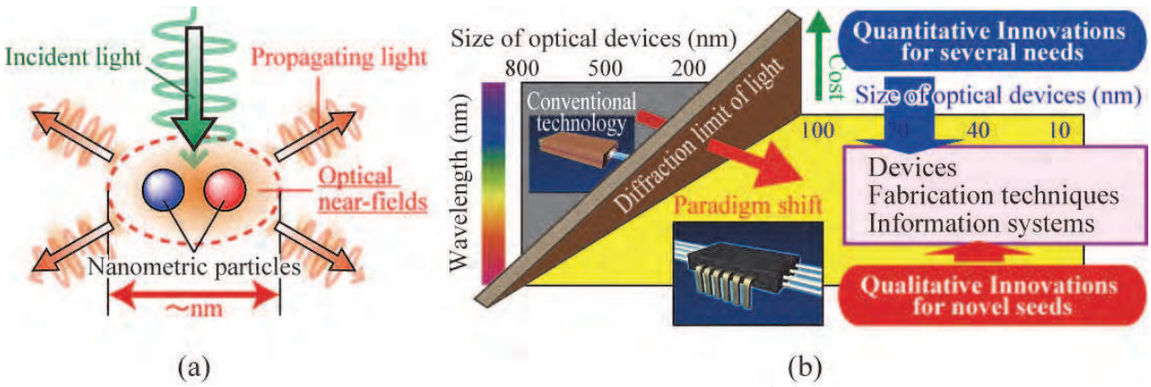


Fig. 1. (a) Generation of optical near-fields, and (b) development of nanophotonics. Because optical near-fields do not involve the optical diffraction limit and they exhibit characteristic features that depend on direct interaction with materials, both *quantitative* and *qualitative* innovations can be achieved.

2.2 Hierarchy based on nanophotonics

Hierarchy in optical near-fields is one of the most appealing attributes for making innovative devices and systems based on nanophotonics. Naruse et al. investigated the hierarchy within the scale of optical near-fields, whose distribution is represented by a Yukawa function (Ohtsu et al., 2008), by investigating the size of materials and their associated optical near-fields (Naruse et al., 2005). The optical near-field response at a given scale is the result of interactions between the retrieval probe and the nanometric materials, and it is correlated with the materials involved at that scale. This feature has been exploited in various applications, for example, hierarchical optical memories where shape-engineered nanostructures provide two-layer responses in optical near-fields (Naruse et al., 2008). Moreover, besides the sizes of the materials, the shape, alignment, and composition are also important physical properties for engineering hierarchical systems. By suitable arrangement of such properties, several characteristic distributions of optical near-fields can be revealed (Naruse et al., 2008; Tate et al., APB2009; Tate et al., OptExp2009). These characteristics exert a large influence on the retrieval, and it means that various retrieval layers can be independently implemented in the same device in the form of a *nanophotonic hierarchical system* (Fig. 2).

From the point of view of the optical security, each layer is defined as an independent information layer. This enables a security layer structure in which nano-scale layers implement covertness and macro-scale layers implement overtness. The former is technically difficult to access and is non-duplicatable, whereas the latter is easy to access and is mass-producable.

3. Nanophotonic hierarchical hologram

3.1 Concept

We can see the hierarchy of optical near-fields and far-fields because optical near-field interactions are distinguishable with propagating light. This characteristic feature has led to hierarchical optical system designs, such as *nanophotonic hierarchical holograms* (Tate et al., 2008), where independent functions are associated with both optical near- and far-fields in the same device. Figure 3 shows the basic concept of the hierarchical hologram.

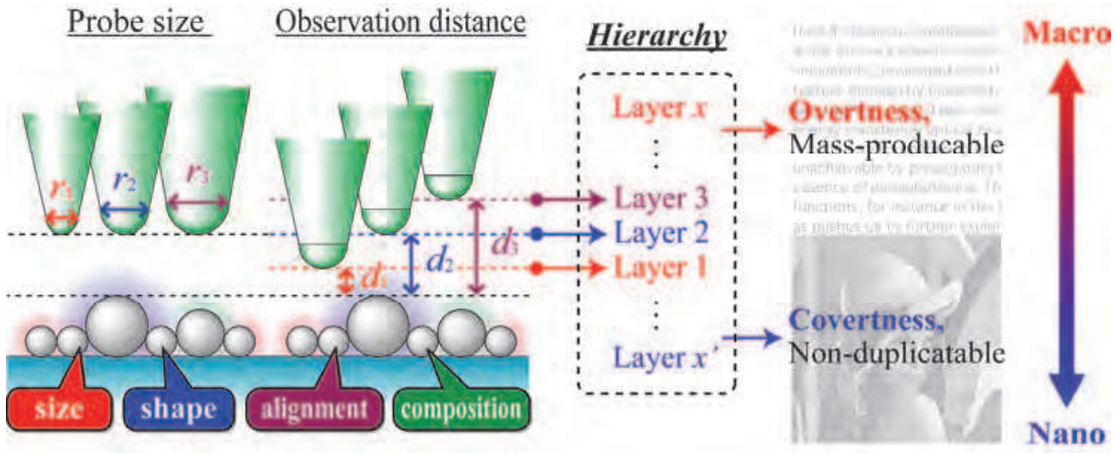


Fig. 2. Conceptual image of hierarchy based on nanophotonics, and innovative optical security system utilizing the hierarchical structure. The important point is that, because induced optical near-fields are the result of interactions between nanometric structures, the hierarchical property can be designed by adjusting the size, shape, alignment, and composition of the nanometric structures.

In a nanophotonic hierarchical hologram, the physical scale of the nanometric structural changes is less than 100 nm, whereas the physical scale of the elemental structures of the hologram is larger than 100 nm. In principle, a structural change occurring at the subwavelength scale does not affect the optical response function, which is dominated by propagating light. Therefore, the visual aspect of the hologram is not affected by such a small structural change on the surface. Additional data can thus be written by engineering structural changes in the subwavelength regime so that they are only accessible via optical near-field interactions (we call this *near-mode* retrieval) without having any influence on the optical response obtained via the conventional far-field light (what we call *far-mode* retrieval). By applying this hierarchy, new functions can be added to conventional holograms.

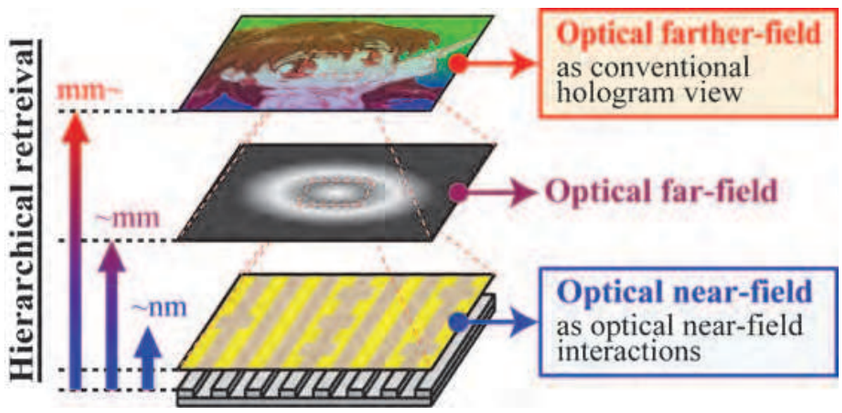


Fig. 3. Basic concept of functional hierarchy of nanophotonic hierarchical hologram. In principle, no interference occurs between each layer, because optical near-field interactions are distinguishable from the conventional hologram view, which consists of diffracted propagating light.

3.2 Near-field – Far-field hierarchy

First of all, in actual use of the hierarchical hologram, it is necessary to demonstrate that a nanometric structural change does not affect the optical response in the far-mode retrieval. To verify this, 500 nm-pitch Si diffraction gratings, in which nanometric depressions were embedded in the grid structures as near-mode data, were fabricated by using electron-beam (EB) lithography. A single isolated depression and multiple periodic depressions were embedded in each grating, as shown in Fig. 4(a) and (b), respectively. The size of each depression was less than 50 nm. The fabricated diffraction gratings were illuminated by the light from a He-Ne laser (λ = 633 nm), and the intensity of each diffracted beam was measured. Figure 4(c) shows the diffracted light pattern from the grating with periodic depressions. Large regular diffraction spots due to the grid structure and a number of tiny spots due to the periodic depressions were observed in the diffraction pattern. The diffraction efficiencies of each order of diffraction spots for each grating, calculated from the measured optical intensity of each spot, are shown in Fig. 4(d). The first-order diffraction efficiencies of a grating with no embedded depressions, the grating with the isolated depression, and the grating with the periodic depressions were 9.8 %, 9.7 %, and 10.3 %, respectively, showing a relative difference of less than 10 % between gratings with and without embedded depressions. No large differences were evident in the other diffraction orders either. This result shows that embedding the nanometric fabricated structures did not have a large effect on the function of conventional optical devices, that is, on their far-mode retrieval.

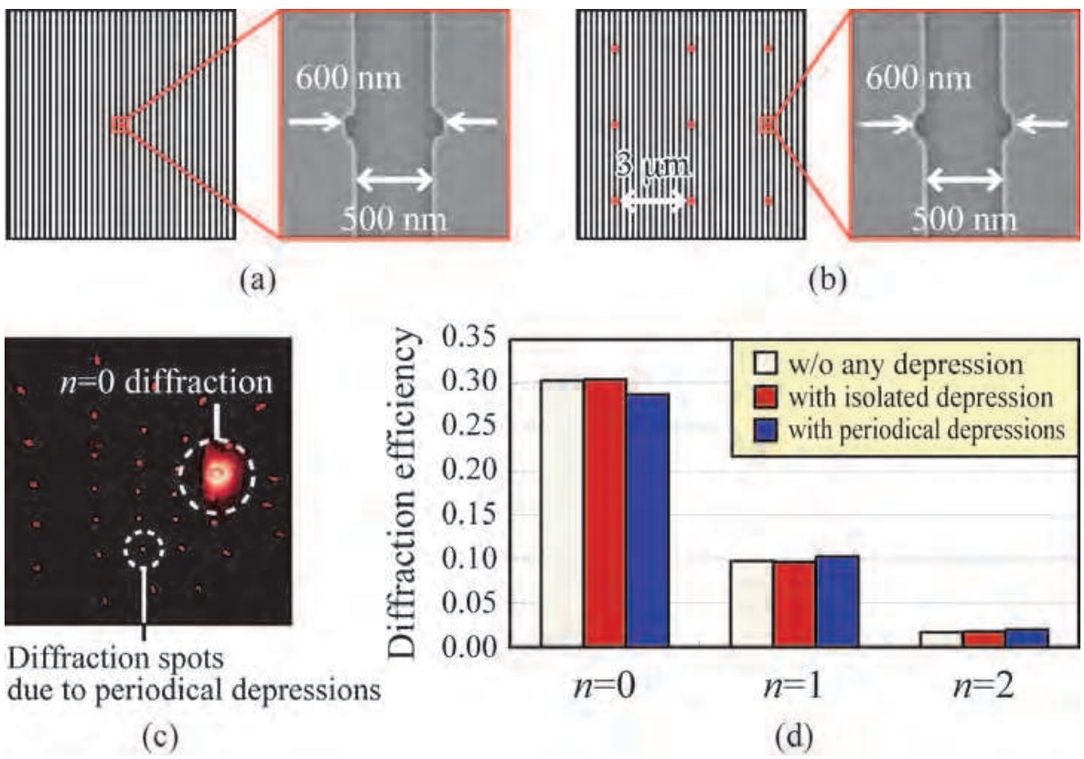


Fig. 4. SEM images of fabricated gratings with (a) single isolated depression and (b) multiple periodic depressions. (c) Diffraction pattern from the grating with periodic depressions. (d) Compared diffraction efficiencies of each grating, where *n* represents the diffraction order.

3.3 Retrieval of nanophotonic code

For a practical demonstration of near-mode retrieval, the pattern of induced optical near-fields generated by irradiating an embedded nanometric structure with light is defined as a *nanophotonic code*. An optical near-field is a non-propagating light field generated in a space extremely close to the surface of a nanometric structure. Because the light distribution depends on several parameters of the structure and the retrieval setup, various types of coding can be considered. Moreover, several novel features of nanophotonics, such as energy transfer (Ohtsu et al., 2008) and hierarchy (Naruse et al., 2005), may be exploited to achieve further functional improvements of nanophotonic codes.

As shown in Fig. 5, we created a sample device to experimentally demonstrate the retrieval of a nanophotonic code within a hologram. The entire device structure, whose size was 15 mm × 20 mm, was fabricated by EB lithography on a Si substrate, followed by sputtering a 50 nm-thick Au layer, as schematically shown in the cross-sectional profile in Fig. 5.

Our prototype device was essentially based on the design of Virtuagram®, developed by Dai Nippon Printing Co., Ltd., Japan, which is a high-definition computer-generated hologram composed of binary-level one-dimensional modulated gratings. As indicated in the left-hand side of Fig. 5, we could observe a three-dimensional image of the earth from the device. Within the device, we formed slightly modified square or rectangular nanometric structures embedded in the original hologram structure, so that near-mode information carried by the nanometric structures was accessible only via optical near-field interactions. The unit size of each embedded structure ranged from 40 nm to 160 nm. For comparison, they were embedded both outside and inside the grid structures, as shown in Fig. 6(a) and (b), respectively.

Note that the original hologram was composed of arrays of one-dimensional grid structures, extending along the vertical direction in Fig. 6 (a). To embed the nanometric structures, the grid structures were partially modified in order to implement the nanophotonic codes. Nevertheless, the grid structures remained topologically continuously connected along the vertical direction. On the other hand, the nanophotonic codes were always isolated from the continuous original grid structures. These geometrical characteristics produce interesting polarization dependence, which is discussed in detail in Sec. 3.3.1.

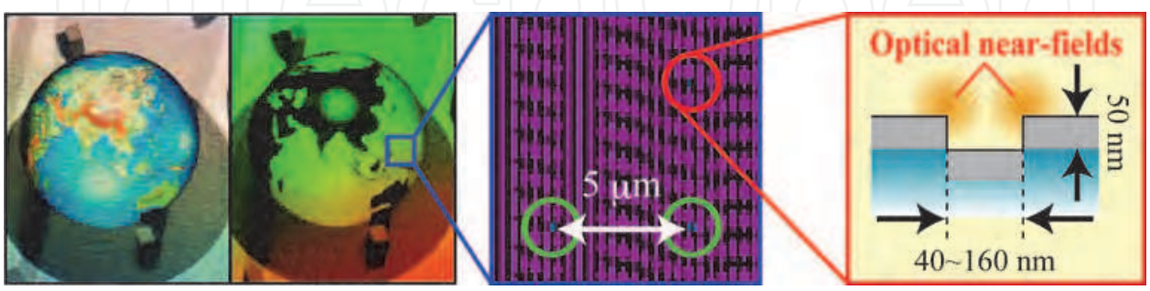


Fig. 5. Schematic diagram of the sample device for demonstration of nanophotonic hierarchical hologram with a nanophotonic code embedded within the embossed structure of Virtuagram®.

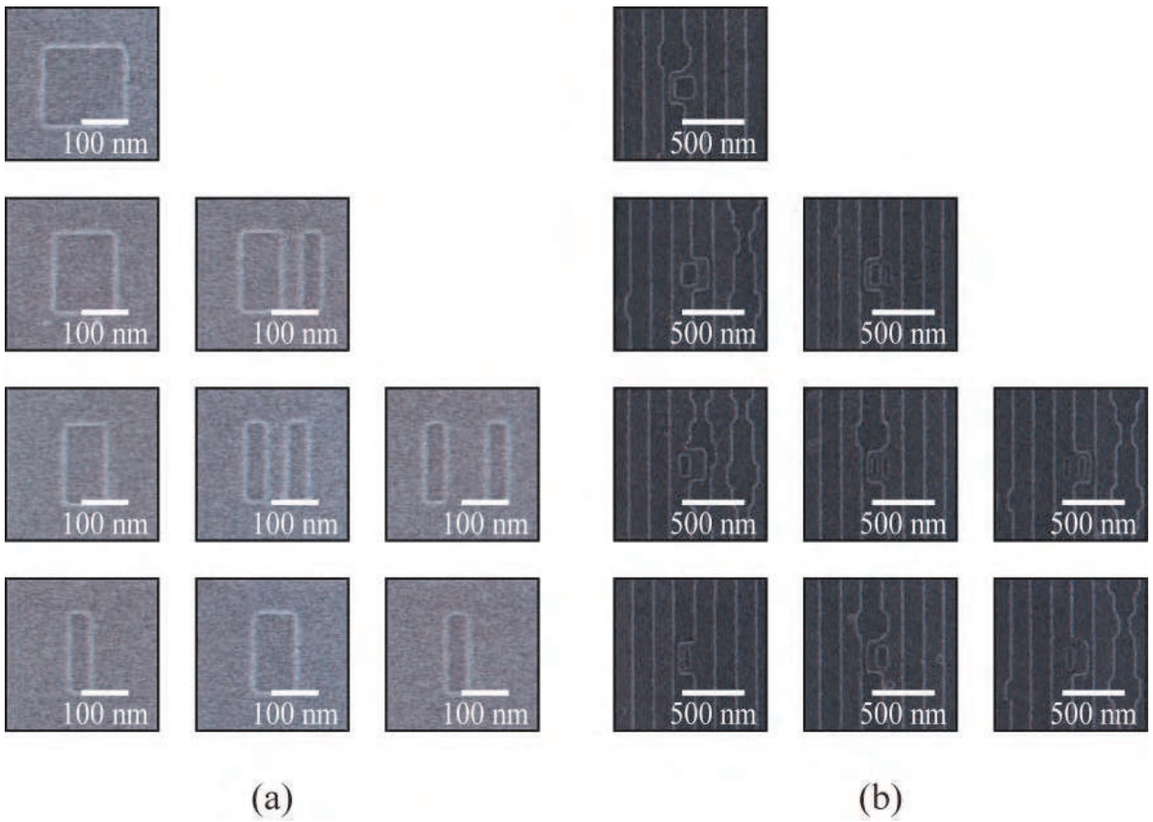


Fig. 6. SEM images of embedded nanometric structures (a) outside and (b) inside the grid structures of the original hologram.

3.3.1 Numerical evaluations

Before conducting the experimental demonstration with fabricated samples, the electric fields at the surfaces of nanometric structures were numerically calculated by the finite-difference time-domain (FDTD) method. As shown in Figs. 7, two types of calculation models were created in order to examine polarization dependency in retrieving the nanophotonic code. The embedded nanometric structure was represented by a square aperture whose side length was 150 nm, shown near the centre of the model. On the other hand, in the model shown in Fig. 7(b), the pitch of the periodic one-dimensional wire-grid structure was 150 nm, and the depth was 100 nm, which models the typical structure of an embossed hologram, and an aperture of the same size as that in Fig. 7(a) was embedded. The material of structures was assumed to be Au, and the structures were assumed to be irradiated with polarized plane waves coming from far above the structures. The wavelength was set to 785 nm. Periodic-conditioned computational boundaries were located 1.5 μm away from the center of the square-shaped aperture. By comparing those two cases, we can predict the effect of the existence of grid structures serving as the environmental structures on nanophotonic code retrieval. Also, we chose the square-shaped structure, which is isotropic in both the x and y directions in order to clearly evaluate the effects of the environmental structures and ignore the polarization dependency originating in the structure of the nanometric aperture itself.

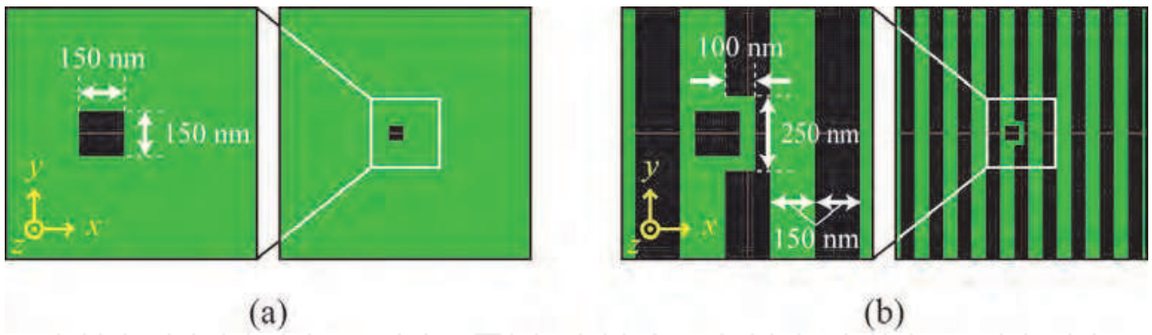


Fig. 7. Calculation model of embedded nanometric structure (a) without and (b) with environmental grid structure.

Figure 8(a), (c) and (b), (d) show calculated electric field intensity distributions on the surfaces of the structures assuming *x*-polarized and *y*-polarized input light irradiation to each model, respectively. As shown, although the model *without* the grid structure did not reveal any polarization dependency, the model *with* the grid structure revealed evident polarization dependency for the *x*- and *y*-polarized irradiation. Moreover, enhanced electric field intensity was obtained with *x*-polarized irradiation to the model with the grid structure.

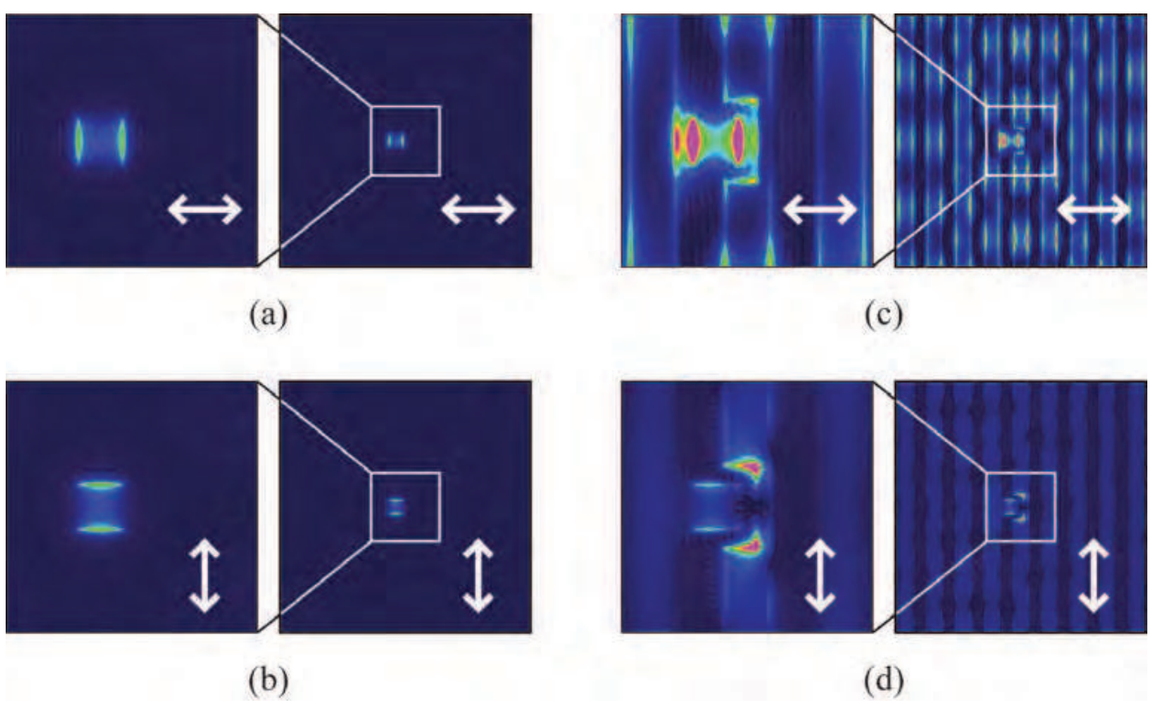


Fig. 8. Calculated intensity distribution of electric field produced by (a), (c) *x*-polarized light and (b), (d) *y*-polarized light input to the models without ((a), (b)) and with ((c), (d)) the grid structures.

In order to quantitatively investigate how the environmental grid structure affected the electric field in the vicinity of the nanometric structure and the influence of input light polarization, the average electric field intensity was evaluated in the area of the nanometric structure, denoted by $\langle I \rangle_{\text{code}}$. The average electric field intensity in the area including the surrounding areas is denoted by $\langle I \rangle_{\text{env}}$. More specifically, $\langle I \rangle_{\text{code}}$ represents the average electric field intensity in the 0.6 μm × 0.6 μm area covering the nanophotonic code, as shown by the dotted square in Fig. 9(a), whereas $\langle I \rangle_{\text{env}}$ indicates that in the 2.5 μm × 2.5 μm area indicated by the dashed square in Fig. 9(a). Figure 9(b) summarizes the calculated values of $\langle I \rangle_{\text{code}}$ and $\langle I \rangle_{\text{env}}$ with each model, respectively shown by the left and right bars.

First, the polarization dependencies are investigated. As shown in Fig. 8, in the case of the nanometric structure embedded in the environmental grid structure, evident polarization dependency was observed for both $\langle I \rangle_{\text{code}}$ and $\langle I \rangle_{\text{env}}$ in Fig. 9(b), too. Figure 9(c) compares the ratio of $\langle I \rangle_{\text{code}}$ with *x*-polarized input light to that with *y*-polarized input light for the embedded and isolated structures. As shown, $\langle I \rangle_{\text{code}}$ with *x*-polarized input light was about two times larger than $\langle I \rangle_{\text{code}}$ with *y*-polarized input light. On the other hand, the isolated nanometric structure did not show any polarization dependency.

Second, from the viewpoint of facilitating recognition of the nanophotonic code embedded in the hologram, it is important to obtain a kind of higher *recognizability* for the signals associated with the nanometric structures. In order to evaluate this recognizability, here we define a numerical figure-of-merit R_{num} as

$$R_{\text{num}} = \frac{\langle I \rangle_{\text{code}}}{\langle I \rangle_{\text{env}}} \times \langle I \rangle_{\text{code}}, \tag{1}$$

which yields a higher value with higher contrast with respect to $\langle I \rangle_{\text{code}}$ and $\langle I \rangle_{\text{env}}$ (indicated by the term $\langle I \rangle_{\text{code}} / \langle I \rangle_{\text{env}}$) and with higher signal intensity (indicated by $\langle I \rangle_{\text{code}}$). Figure 9(d) shows the calculated R_{num} in the case of *y*-polarized light input to thetwo types of models. The result indicates that the nanometric structure embedded in the environmental grid structure is superior to that of the isolated structure in terms of the recognizability defined by eq. (1), as shown in Figure 9.

We consider that such polarization dependency and enhanced recognizability are due to the environmental grid structure that extends along the vertical direction. The input light induces oscillating surface charge distributions due to coupling between the light and electrons in the metal. The *y*-polarized input light induces surface charges along the vertical grid; since the grid structure continuously exists along the *y*-direction, there is no chance for the charges to be concentrated. However, in the area of the embedded nanometric structure, there is a structural discontinuity in the grid; this results in higher charge concentration only at the edges of the embedded nanometric structure. On the other hand, the *x*-polarized input light sees structural discontinuity along the horizontal direction due to the vertical grid structure, as well as in the areas of the embedded structures. It turns out that charge concentration occurs not only in the edges of the embedded structures but also at other horizontal edges of the environmental grid structure. Therefore, by comparing this with the *y*-polarized model, enhancement of the electric field intensity and its polarization dependency is evident. In contrast to these nanometric structures embedded in holograms,

for the isolated square apertures, both the *x*-polarized input light and the *y*-polarized input light have equal effects on the nanostructures.
These mechanisms indicate that such nanophotonic codes embedded in holograms could also exploit these polarization and structural dependences, not only for retrieving near-mode information via optical near-field interactions. For instance, we could facilitate near-mode information retrieval using suitable input light polarization and environmental structures.

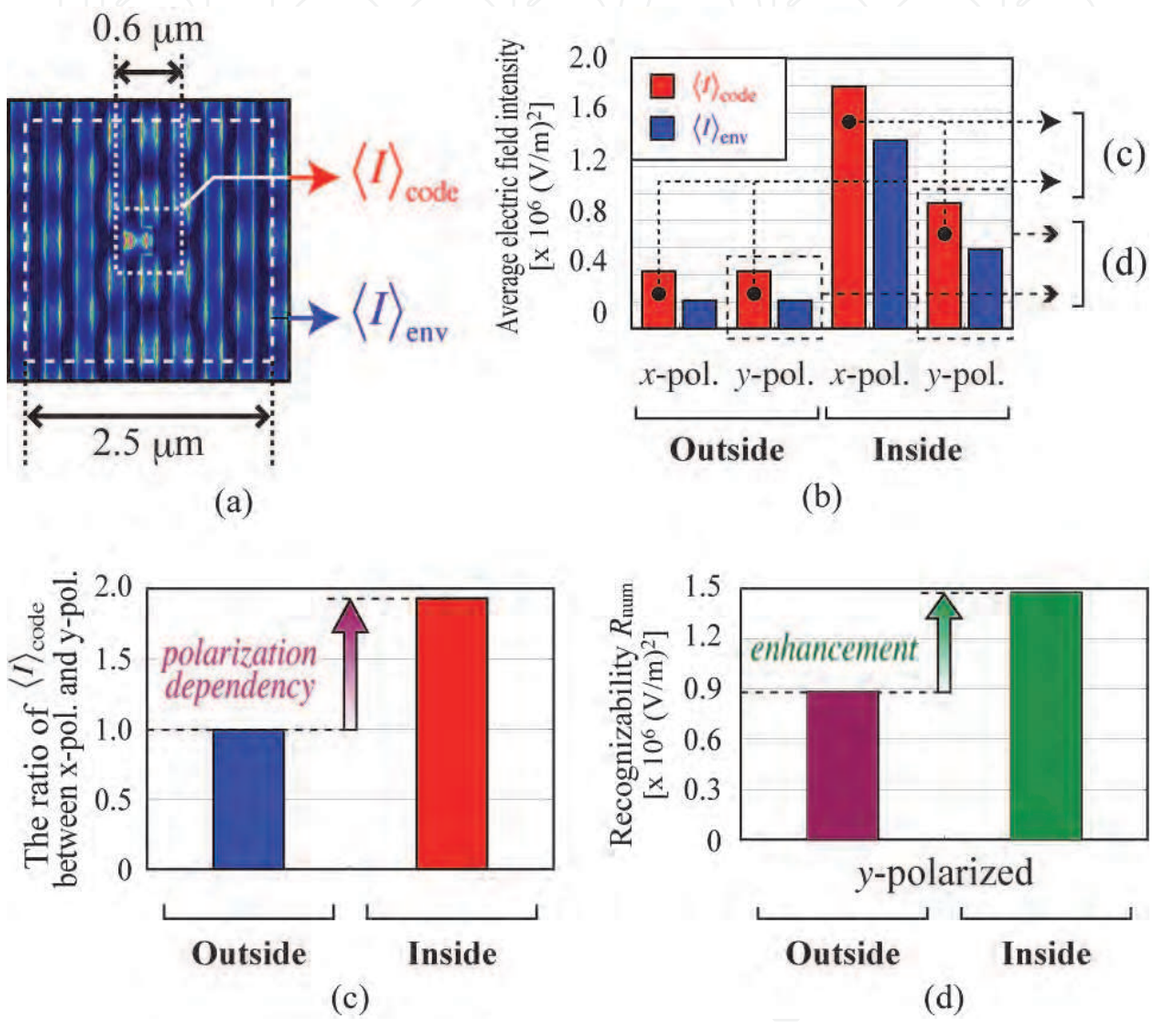


Fig. 9. (a) Schematic diagram explaining definition of average electric field intensities $\langle I \rangle_{\text{code}}$ and $\langle I \rangle_{\text{env}}$, and (b) their graphical representations in each calculation model. Evident polarization dependency was exhibited in the case of the nanometric code embedded in environmental structures. (c) The ratio of $\langle I \rangle_{\text{code}}$ with *x*-polarized input light to that with *y*-polarized input light for the embedded and isolated structures. (d) Numerical visibility R_{num} in two types of models with *y*-polarized input light. The result indicates that the visibility of the nanophotonic code was greatly enhanced by embedding it in the environmental structure.

3.3.2 Experimental demonstration

In the experimental demonstration, the optical responses of sample devices, shown in Figs. 6, during near-mode observation were detected using a near-field optical microscope (NOM). A schematic diagram of the detecting setup is shown in Fig. 10. The NOM was operated in an illumination-collection mode with a near-field probe having a tip with a radius of curvature of 5 nm. The fiber probe was connected to a tuning fork. Its position was finely regulated by sensing a shear force with the tuning fork, which was fed back to a piezoelectric actuator of the probe stage. The observation distance between the tip of the probe and the sample device was set at less than 50 nm. The light source used was an LD with an operating wavelength of 785 nm, and scattered light was detected with a photomultiplier tube (PMT). A Glan-Thompson polarizer (extinction ratio 10^{-6}) selected only linearly polarized light as the radiation source, and a half-wave plate (HWP) rotated the polarization.

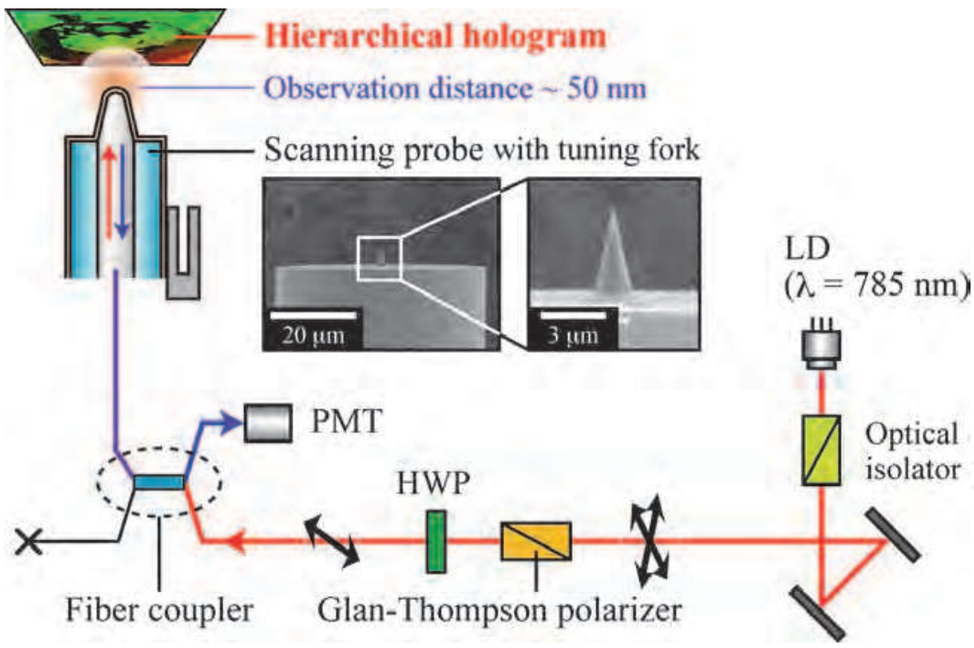


Fig. 10. Schematic diagram of the experimental setup for retrieving a nanophotonic code.

Figures 11(a) and (b) show retrieved results of nanophotonic codes that were outside and inside the environmental grid structures of the hologram, respectively, using a linearly polarized radiation source rotated by 0 degree to 180 degree at 20-degree intervals. As is evident in Fig. 11(a), although small and noisy intensity distributions were obtained, clear polarization dependence was observed in Fig. 11(b); for example, from the area of the nanophotonic code located in the center, a high-contrast signal intensity distribution was obtained with polarizations around 80 degree.

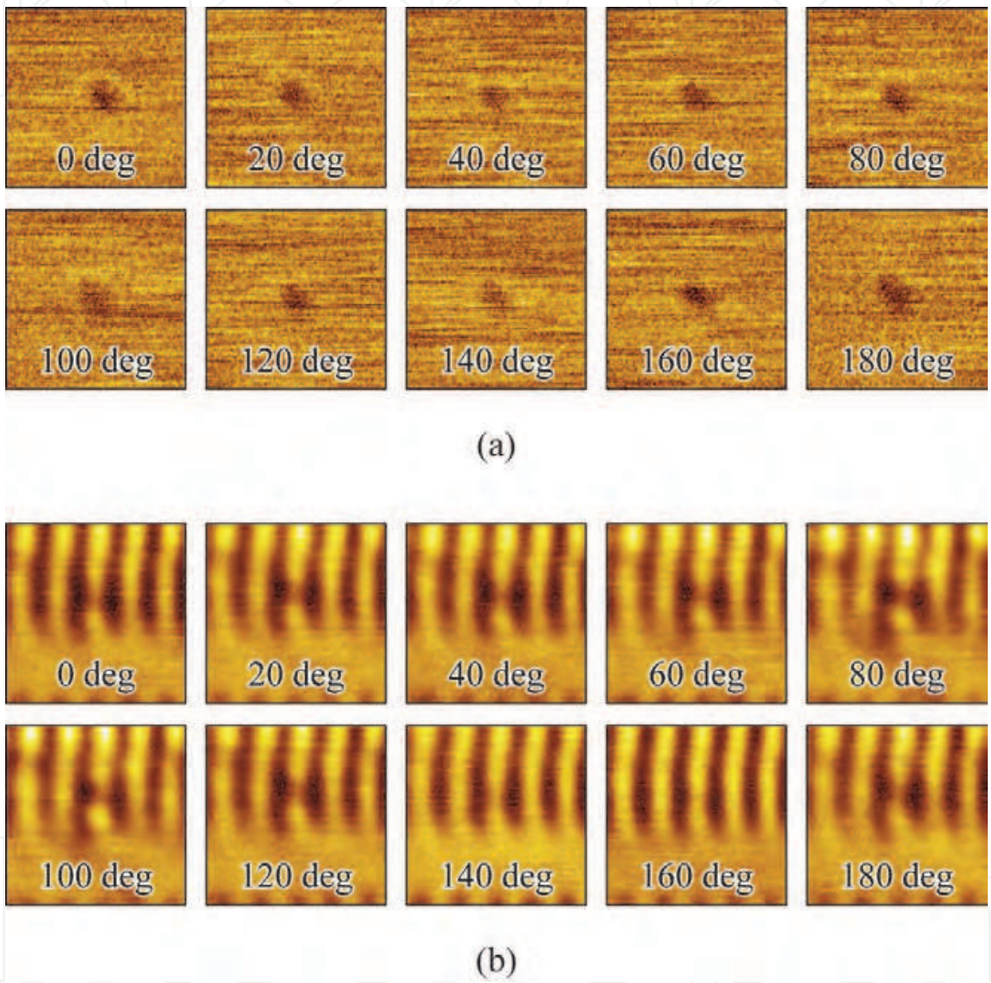


Fig. 11. Observed NOM images of optical intensity distributions of retrieved nanophotonic codes (a) outside and (b) inside the environmental grid structure.

To quantitatively evaluate the characteristics of the embedded nanophotonic code, we investigated two kinds of intensity distribution profiles from the observed NOM images. One is a horizontal intensity profile along the dashed line in Fig. 12(a), which crosses the area of the nanophotonic code, denoted by $I(x)$, where x represents the horizontal position. The other was also an intensity distribution as a function of horizontal position x; however, at every position x, we evaluated the average intensity along the vertical direction within a range of 2.5 μm, denoted by $\langle I(x) \rangle_{\text{env}}$, which indicates the environmental signal

distribution. When a higher intensity is obtained selectively from the area of the nanophotonic code, the difference between $I(x)$ and $\langle I(x)\rangle_{\text{env}}$ can be large. On the other hand, if the intensity distribution is uniform along the vertical direction, the difference between $I(x)$ and $\langle I(x)\rangle_{\text{env}}$ should be small. Thus, the difference between $I(x)$ and $\langle I(x)\rangle_{\text{env}}$ indicates the visibility of the nanophotonic code. We define an experimental recognizability R_{exp} as

$$R_{\text{exp}} = \sum_{x} \left| I(x) - \langle I(x)\rangle_{\text{env}} \right| . \tag{2}$$

Figures 12(b) shows R_{exp} as a function of input light polarization based on the NOM results shown in Figure 11.

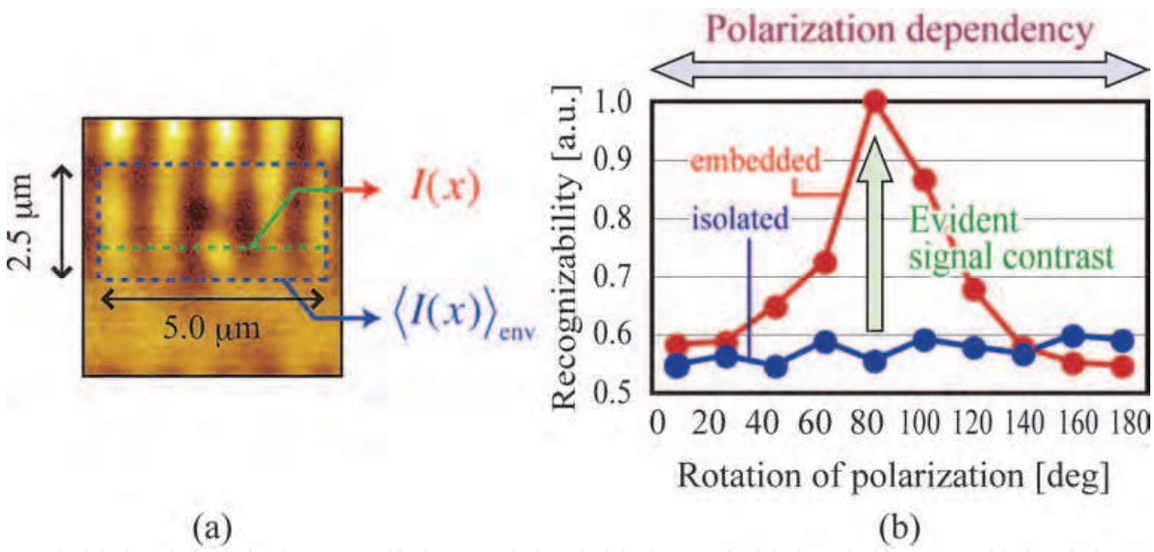


Fig. 12. (a) Definition of $I(x)$ and $\langle I(x)\rangle_{\text{env}}$ for numerical evaluation, and (b) calculated experimental recognizability, R_{exp}, of embedded nanometric structure (red curve) and that of isolated nanometric structure (blue curve). Evident recognizability and polarization dependency were exhibited.

The nanophotonic code embedded in the hologram exhibited much greater polarization dependency, as indicated by *embedded* in Fig. 12(b), where the maximum $R_{\exp}$ was obtained at 80-degree input polarization. On the other hand, only slight polarization dependency was observed with the isolated nanophotonic code, as indicated by *isolated*. These characteristics of retrieving the nanophotonic code in the environmental grid structure agree well with the numerical results in Fig. 9.

4. Summary

In this chapter, we described the basic concept of a nanophotonic hierarchical hologram and a nanophotonic code embedded in a hologram as an implementation of a hierarchical hologram. One of the most notable characteristics of our proposed approach is embedding a nanophotonic code within the patterns of a hologram composed of one-dimensional grid structures; it yields clear polarization dependence compared with an isolated nanophotonic code that is not embedded within a grid structure. These features were successfully demonstrated both numerically and experimentally.

In future research, the relation between the retrieved optical intensity distributions and the design of the nanometric structures may come to be understood, including their environmental conditions. Such insights should allow us to propose, for instance, an optimized strategy for implementing nanophotonic codes, or a strategy that is robust against errors that possibly occur in the fabrication and/or retrieval processes (Naruse et al., 2009).

From the point of view of practical use of these concepts in novel security devices, because embedding and retrieval of a nanophotonic code require highly advanced technical know-how, this approach can also improve the strength of anti-counterfeiting measures. The number of layers can be increased in the near-mode observation to further extend the hierarchical function. The optical near-field interaction between multiple nanometric structures produces a characteristic spatial distribution depending on the size, alignment, etc. Therefore, various optical signal patterns can be observed depending on the size of the fiber probe, and another layer can be added in near-mode observation (Naruse et al., 2007; Naruse et al., 2005). A simpler method for achieving such a hierarchical function is required, without using optical fiber probe tips. The scale for such retrieval might be set at the submillimeter range, as represented by *optical far-field* in Fig. 3. These aspects are currently being investigated by the authors.

Finally, the concept of hierarchy based on nanophotonics may produce innovations not only in optical security but also for other optical applications, such as lenses and jewellery. Adding extra functions in this way creates value-added media with only a slight impact on the primary functions. However, a trade-off occurs between the nanometric fabrication conditions (e.g., size and pitch) and the impact on the primary functions. Adequate discussion is needed to investigate these trade-offs in each application for their practical use.

5. Acknowledgments

This work was supported in part by a comprehensive program for personnel training and industry–academia collaboration based on projects funded by the New Energy and Industrial Technology Development Organization (NEDO), Japan, the Global Center of

Excellence (G-COE) Secure-Life Electronics project, and Special Coordination Funds for Promoting Science and Technology sponsored by the Ministry of Education, Culture, Sports, Science and Technology (MEXT), Japan.

6. References

Lorenzi, R. (2010). Do Mona Lisa' s eyes hide a secret code?, *Discovery News*, 13 December

Javidi, B. & Horner, J. L. (1994). Optical pattern recognition for validation and security verification, *Optical Engineering*, Vol. 33, pp. 1752-1756, 1994

Refregier, P. & Javidi, B. (1995). Optical image encryption based on input plane and Fourier plane random encoding, *Optics Letters*, Vol. 20, pp. 767-769, 1995

Rakuljic, G. A., Leyva, V., & Yariv, A. (1992). Optical data storage by using orthogonal wavelength-multiplexed volume holograms, *Optics Letters*, Vol. 17, pp. 1471-1473, 1992

Van Renesse, R. L. (1998). *Optical document scanning*, Altech House Optoelectronics Library, 1998

McGrew, S. P. (1990). Hologram counterfeiting: problems and solutions, *Proceedings of SPIE*, *Optical Security and Anticounterfeiting Systems*, Vol. 1210, pp. 66-76, 1990

Zhdanov, G. S., Libenson, M. N., & Martsinovskii, G. A. (1998). Optics in the diffraction limit: principles, results, and problems, *Physics-Uspekhi*, Vol. 41, pp. 719-722, 1998

Ohtsu, M., Kobayashi, K., Kawazoe, T., Yatsui, T., & Naruse, M. (2008). *Principles of Nanophotonics*, Taylor and Francis, Boca Raton, 2008

Tate, N., Nomura, W., Yatsui, T., Naruse, M., & Ohtsu, M. (2008). Hierarchical hologram based on optical near- and far-field responses, *Optics Express*, Vol. 16, pp. 607-612, 2008

Tate, N., Naruse, M., Yatsui, T., Kawazoe, T., Hoga, M., Ohyagi, Y., Fukuyama, T., Kitamura, M., & Ohtsu, M. (2010). Nanophotonic code embedded in embossed hologram for hierarchical information retrieval, *Optics Express*, Vol. 18, pp. 7497-7505, 2010

Ozbay, E. (2006). Plasmonics: Merging Photonics and Electronics at Nanoscale Dimensions, *Science*, Vol. 311, pp. 189-193, 2006

Nishida, T., Matsumoto, T., Akagi, F., Hieda, H., Kikitsu, A., & Naito, K. (2007). Hybrid recording on bit-patterned media using a near-field optical head, *Journal of Nanophotonics*, Vol. 1, 011597, 2007

Naruse, M., Yatsui, T., Nomura, W., Hirose, N., & Ohtsu, M. (2005). Hierarchy in optical near-fields and its application to memory retrieval, *Optics Express*, Vol. 13, pp. 9265-9271, 2005

Naruse, M., Yatsui, T., Kawazoe, T., Tate, N., Sugiyama, H., & Ohtsu, M. (2008). Nanophotonic Matching by Optical Near-Fields between Shape-Engineered Nanostructures, *Applyed Physics Express*, Vol. 1, 112101, 2008

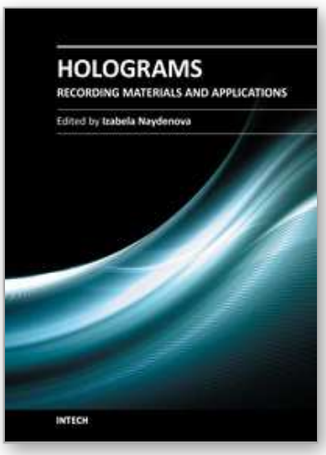
Tate, N., Sugiyama, H., Naruse, M., Nomura, W., Yatsui, T., Kawazoe, T., & Ohtsu, M. (2009). Quadrupole-Dipole Transform based on Optical Near-Field Interactions in Engineered Nanostructures, *Optics Express*, Vol. 17, 11113, 2009

Tate, N., Nomura, W., Yatsui, T., Naruse, M., & Ohtsu, M. (2009). Hierarchy in optical near-fields based on compositions of nanomaterials, *Applied Physics B*, Vol. 96, pp. 1-4, 2009

Naruse, M., Inoue, T., & Hori, H. (2007). Analysis and Synthesis of Hierarchy in Optical Near-Field Interactions at the Nanoscale Based on Angular Spectrum, *Japanese Journal of Applied Physics*, Vol. 46, pp. 6095-6103, 2007

Naruse, M., Hori, H., Kobayashi, K., Ishikawa, M., Leibnitz, K., Murata, M., Tate, N., & Ohtsu, M. (2009). Information theoretical analysis of hierarchical nano-optical systems in the subwavelength regime, *Journal of the Optical Society of America B*, Vol. 26, pp. 1772-1779, 2009

IntechOpen



Holograms - Recording Materials and Applications

Edited by Dr Izabela Naydenova

ISBN 978-953-307-981-3
Hard cover, 382 pages
Publisher InTech
Published online 09, November, 2011
Published in print edition November, 2011

Holograms - Recording Materials and Applications covers recent advances in the development of a broad range of holographic recording materials including ionic liquids in photopolymerisable materials, azo-dye containing materials, porous glass and polymer composites, amorphous chalcogenide films, Norland optical adhesive as holographic recording material and organic photochromic materials. In depth analysis of collinear holographic data storage and polychromatic reconstruction for volume holographic memory are included. Novel holographic devices, as well as application of holograms in security and signal processing are covered. Each chapter provides a comprehensive introduction to a specific topic, with a survey of developments to date.

How to reference

In order to correctly reference this scholarly work, feel free to copy and paste the following:

Naoya Tate, Makoto Naruse, Takashi Yatsui, Tadashi Kawazoe, Morihisa Hoga, Yasuyuki Ohyagi, Yoko Sekine, Tokuhiro Fukuyama, Mitsuru Kitamura and Motoichi Ohtsu (2011). Nanophotonic Hierarchical Holograms: Demonstration of Hierarchical Applications Based on Nanophotonics, Holograms - Recording Materials and Applications, Dr Izabela Naydenova (Ed.), ISBN: 978-953-307-981-3, InTech, Available from: http://www.intechopen.com/books/holograms-recording-materials-and-applications/nanophotonic-hierarchical-holograms-demonstration-of-hierarchical-applications-based-on-nanophotonic

INTECH
open science | open minds

InTech Europe
University Campus STeP Ri
Slavka Krautzeka 83/A
51000 Rijeka, Croatia
Phone: +385 (51) 770 447
Fax: +385 (51) 686 166
www.intechopen.com

InTech China
Unit 405, Office Block, Hotel Equatorial Shanghai
No.65, Yan An Road (West), Shanghai, 200040, China
中国上海市延安西路65号上海国际贵都大饭店办公楼405单元
Phone: +86-21-62489820
Fax: +86-21-62489821

© 2011 The Author(s). Licensee IntechOpen. This is an open access article distributed under the terms of the Creative Commons Attribution 3.0 License, which permits unrestricted use, distribution, and reproduction in any medium, provided the original work is properly cited.

IntechOpen

IntechOpen